HHS Public Access

Author manuscript

J Chem Theory Comput. Author manuscript; available in PMC 2016 December 09.

Published in final edited form as:

J Chem Theory Comput. 2016 November 08; 12(11): 5575–5584. doi:10.1021/acs.jctc.6b00618.

Conserved mechanism of conformational stability and dynamics in G-protein-coupled receptors

Supriyo Bhattacharya, **Romelia Salomon-Ferrer**, **Sangbae Lee**, and **Nagarajan Vaidehi**
Beckman Research Institute, City of Hope National Medical Center, 1500 Duarte Road, Duarte, CA 91010, USA

Abstract

GPCRs are transmembrane receptors involved in diverse biological functions. Despite the diversity in their amino acid sequences, class A GPCRs exhibit a conserved structural topology and possibly common mechanism of receptor activation. To understand how this high sequence diversity translates to a conserved functional mechanism, we have compared the dynamic behavior of eight class A GPCRs comprising of six biogenic amine receptors, and the adenosine A_{2A} and a peptide receptor protease activated receptor 1. Starting from the crystal structures of the inactive state of these receptors bound to inverse agonists or antagonists, we have performed multiple all-atom MD simulations adding up to several microseconds of simulation. We elucidate the similarities and differences in the dynamic behavior and the conformational ensembles sampled by these eight class A GPCRs. Among the six biogenic amine receptors studied here, the β_2 adrenergic receptor shows the highest level of fluctuation in the 6^{th} and 7^{th} transmembrane helices, possibly explaining its high basal activity. In contrast, the muscarinic acetylcholine receptors show the lowest fluctuations as well as tight packing and low hydration of their transmembrane domains. All eight GPCRs show several conserved allosteric communication pipelines from the residues in the agonist binding site with the G protein interface. Positions of the residues along these pipelines that serve as major hubs of allosteric communication are conserved in their respective structures. These findings have important implications in understanding the dynamics and allosteric mechanism of communication in class A GPCRs and hence useful for designing conformation specific drugs.

Graphical abstract

*Corresponding Author: NVaidehi@coh.org.

The authors declare no competing financial interest.

Supporting information

MI convergence (Figure. S1); ionic lock formation during GPCR dynamics simulations (Figure. S2); conserved allosteric pipelines in biogenic amine receptors (Figure. S3); collapsed and open conformations of β_2AR (Figure. S4); packing efficiency of transmembrane hydrophobic residues (Figure. S5); water diffusion into the TM regions of GPCRs during dynamics simulations (Figure. S6); conserved allosteric hubs among class A GPCRs (Figure. S7); list of experimentally mutated residues and their effects (Table S1).

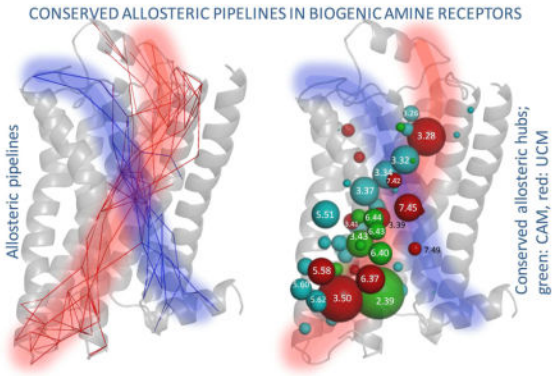

1. INTRODUCTION

G protein coupled receptors (GPCRs) are transmembrane receptors involved in cellular processes and are valuable drug targets. Agonist bound GPCRs have a higher propensity to bind intracellular proteins (such as G-proteins and arrestins) leading to receptor activation and intracellular (IC) signaling, while inverse agonists inhibit receptor activation. Under physiological conditions, GPCRs are highly dynamic and therefore can adopt multiple functional conformational states [1], each of which can couple to different intracellular proteins leading to diverse signaling pathways. Understanding of how the dynamics of various GPCRs populate various conformational functional states is a complex process.

GPCRs share a common topology with seven transmembrane (TM) helices, connected by intra and extracellular loops. The canonical mode of GPCR signaling is through trimeric G proteins, a family of intracellular proteins that bind to the IC interface of the receptor upon activation. The activation of GPCRs is triggered by a combination of conformational selection as well as induced fit upon agonist binding where the intracellular (IC) part of TM6 moves outward from the receptor core, opening a cavity for G protein interaction [2]. Depending on the nature of the agonist binding in the extracellular surface of the GPCR, the receptor binds and activates different G-proteins or other proteins such as β-arrestin. Therefore the agonist/GPCR pair influences the selection of the intracellular protein to which the receptor couples. Since the agonist binding site is located far away from the G-protein coupling interface, the communication between the ligand binding site and IC interface is allosteric in nature [3]. Key residues in the TM domain located in between the ligand binding site and the IC interface have to mediate the allosteric communication between the two domains [4], however weak or strong the allosteric communication may be. Besides, allosteric communication between the residues in the ligand binding site to those in the IC interface is necessary to maintain the receptor in the inactive state when bound to an antagonist or an inverse agonist. Despite being diverse in amino acid sequence identity, class A GPCRs show a conserved structural topology and possibly a common mode of activation. Our hypothesis is that if class A GPCRs have a common mode of activation, then the residues that are involved in receptor activation or deactivation should be located in the same position in their respective three dimensional structures even if the amino acid sequence is not conserved at these positions. Thus, comparing the dynamic behavior across GPCRs can

provide insights into the relative population of various conformational substates that are sampled in the presence of antagonists and the residues that contribute to maintaining the receptor in its inactive conformational state.

Among the class A GPCRs, the biogenic amine receptor family modulate diverse physiological functions, ranging from cardiovascular regulation, neurotransmission, to digestion, sleep and brain activity. The activation of biogenic amine receptors is modulated by chemically similar small molecule agonists that consist of a protonated charged nitrogen. The structure and function of the adrenergic and muscarinic acetylcholine receptors have been extensively studied in the literature using mutagenesis and biophysical methods [3b, 5]. These studies have revealed the functionally important (involved in receptor activation) conserved amino acid sequence motifs within the TM domains of multiple GPCRs, such as the WxP motif on TM6 and the NPxxY motif on TM7. However, the residues that play an important role in the activation or deactivation of the receptor are not known even in biogenic amine receptors.

Recently, we studied the allosteric communication pathways in the β_2-adrenergic receptor using graph theory based algorithm called "*Allosteer*" and microsecond timescale molecular dynamics (MD) simulations [4b]. These simulations showed that some residues in the ligand binding site of GPCRs show significant correlated motion to the residues in the G-protein binding interface, in the time scale of nanoseconds to microseconds. We also showed that the correlated motion between residues in the ligand binding site to the IC interface is stronger in the antagonist bound receptor state than in the agonist bound state. Using *Allosteer*, we calculated the allosteric communication pathways (which we call allosteric pipelines) from the ligand binding site to the G-protein binding interface. Residues within the allosteric pipelines that propagate the allosteric communication were experimentally shown to affect (enhance or suppress) receptor activation upon mutation in multiple class A GPCRs. These results indicate that the pipelines of allosteric communication that modulate receptor activation could be conserved across multiple receptor species. Please note that allosteric communication in this case refers to correlated motion between distant residues in the timescale of nanoseconds that is not accessible by experiments. This type of correlated motion involves measuring time-resolved changes in torsion angles of distant residues and calculating the correlation among these changes. Such correlated motions are important for stabilizing specific receptor conformations such as the inactive or the active state, since they reduce the degree of freedom of the correlated residues. Concerted movement of residues leading to large conformational changes (e.g. motions that lead to transition from the inactive to the active state) is measured by NMR studies on GPCRs [1, 3b]. These concerted changes that occur in longer time scales in the range of tens of microseconds to hundreds of milliseconds, are also referred to as allosteric communication in the literature. These types of motions are slower (in the timescale of microseconds to milliseconds) and are detectable in NMR and single molecule experiments [1]. Our analysis concerns the former motion (correlated motion in nanoseconds timescale), since this timescale is accessible to MD simulations.

Our aim in this study is to compare the dynamic properties of the biogenic amine receptors in their inactive state with the goal of understanding of the biological properties of these

receptors. We have also compared the dynamics of the biogenic amine receptors to that of other class A GPCRs, that we have studied recently [6] to determine whether such properties are conserved across the class A GPCR family. The inactive state of the GPCR is a functional state and the dynamic properties of the inactive state should provide structural basis for the mechanism by which the inverse agonist or the antagonist maintains the receptor in its inactive state. Towards this goal, we have performed all-atom unbiased MD simulations of six biogenic amine receptors and two other class A GPCRs (non biogenic amine family), starting from the respective crystal structures of their inactive states with inverse agonist or antagonist bound. The receptors that we have studied are β_2 and β_1 adrenergic receptors (β_2AR, β_1AR), dopamine D3 receptor (D_3DR), histamine receptor 1 (H_1R), M_2 and M_3 muscarinic acetylcholine receptors (M_2R, M_3R), protease activated receptor 1 (PAR1) and A_{2A} adenosine receptor (A_{2A}R). In our previous work on β_2AR, we found that there is strong allosteric communication between the ligand binding site and EC domain and the G protein interface in the inactive state of β_2AR and this allosteric communication was substantially weaker in the agonist bound β_2AR [4b]. The residues that modulate this allosteric communication contribute to the stability of the inactive state. Thus by studying the allosteric communication in the inactive states of the different receptors, we can gain insight into the mechanism by which antagonists/inverse agonists suppress activation. In this work, we have compared several key aspects of the receptor dynamics such as the movement of the IC end of TM6, packing of hydrophobic residues in the TM core and penetration of water into the TM regions. We have also shown how the major allosteric communication pipelines are conserved across all eight GPCRs and describe a common mechanism of allosteric communication that keeps the receptor in the inactive state.

2. METHODS

2.1. System preparation

Crystal structures of inverse agonist/antagonist bound GPCRs were downloaded from the PDB databank (www.pdb.org). The pdb IDs of the β_2AR, β_1AR, D_3DR, H_1R, M_2R, M_3R, PAR1 and A_{2A}R crystal structures are: 2RH1, 2VT4, 3PBL, 3RZE, 3UON, 4DAJ, 3VW7 and 3PWH respectively. First the stabilizing proteins such as T4 lysozyme were removed from the structures, and missing loops that are less than 10 residues long were then modeled using MODELLER [7], and the missing side chains were added using MAESTRO (Schrodinger LLC). The long ICL3 was omitted from the simulated protein structures. Also the mutated residues in the crystal structures were mutated back to their wild type sequences using MAESTRO (Schrodinger LLC). The amino and carboxy termini of the receptors were capped using neutral acetyl and N-methyl amide capping groups. The topological parameters of the ligands were derived from the PRODRG server [8], and partial atomic charges were calculated according to the B3LYP/6-31G basis set [9] using Jaguar (Schrodinger LLC). The ligand bound receptors were embedded in a pre-equilibrated 1-palmitoyl-2-oleoyl-sn-glycero-3-phosphocholine (POPC) bilayer of 256 molecules. The lipid molecules were packed around the proteins using the *inflateGRO* methodology of GROMACS [10]. To remove the net charge of the system, Cl- or Na+ ions were added as counter-ions. The SPC water model [11] was used as the solvent for each system.

2.2. MD simulation protocol

The MD simulations were performed using the GROMOS53a6 force field [12] and the software package GROMACS v4.6 [13]. The systems were first minimized until the maximum force became less than 100.0 kJ-mol^{-1}nm^{-1}. The systems were equilibrated in two steps. First, 200 ps of MD simulation was performed on each system, in which the volume was kept constant and the temperature was linearly increased from 0K to 310K. Next, 5 ns of MD simulation was performed in the NPT ensemble at 1 atm pressure and a temperature of 310K. For both these steps, the heavy atoms of the proteins and the ligands were restrained using a force constant of 1000 kJ-mol^{-1}nm^{-1}. Production simulations were initiated from the final snapshots of equilibration step and were performed at a constant pressure of 1 atm and temperature of 310K. The Nose-Hoover thermostat [14] and Parrinello-Rahman barostat [15] were used. For each GPCR, 10 individual simulations were performed with different initial velocities (sampled from the Maxwell-Boltzmann distribution at 310K) lasting for 100ns each using a timestep of 2 fs. A cutoff distance of 12A was used for nonbonded interactions, and PME (particle mesh Ewald) method [16] was used for calculating long range electrostatics.

2.3. Analysis of MD trajectories

The root mean square fluctuation (RMSF) was calculated using the GROMACS package [13], while inter-residue distances were calculated using VMD [17]. To estimate the errorbars in RMSF, the MD trajectories for each receptor was divided into groups of three and the RMSF of each group was calculated separately. This ensured that both the intra-trajectory as well as inter-trajectory fluctuations were captured. These RMSF values were then used for calculating the errorbars. To calculate the vdW packing efficiency for a given pair of residues, we calculated the number of heavy atoms of the two residues that are within 4A of each other for each frame of the MD trajectories. The net vdW packing efficiency was obtained by averaging over all the simulation snapshots. The number of water molecules within 5A of the TM residues were calculated using VMD [17]. The water occupancy profiles within the TM regions were displayed using the volmap module of VMD [17] with a cutoff value of 0.1.

2.4. Calculation of allosteric pipelines

The detailed calculation of the allosteric pipelines is discussed in [4b]. Here we give a brief overview of the method as implemented here. We first calculate the mutual information (MI) in torsional degrees of freedom between each pairs of dihedral angles within each receptor. The average MI between a residue pair is the mean of the pairwise torsion angle MIs between the two residues. Higher the MI, more correlated is the dynamics of the two residues. We next calculated the allosteric pathways between each pair of residues that showed above average MI ($MI > MI_{avg}$) and were farther than 10A in the receptor structure. We first constructed an undirected graph using inter-residue contacts, where the residues formed nodes and the inter-residue contacts formed the edges of the network. An inter-residue contact was identified if the Cα atoms of the residue pair were within 7.5A of one another. The edge weights were proportional to the negative of the MI between the terminal residues of the edge. The allosteric pathway between two residues was calculated as the

shortest pathway that maximizes the sum of the edge weights in a pathway using the algorithm by Dijkstra [18], as implemented in the Bioinformatics ToolBox in MATLAB (The MathWorks, Natick, MA). The top 10% of the allosteric pathways by terminal MI were then clustered into pipelines. To determine the spatial proximity of two pathways, we calculated the pathway "overlap" defined as the fraction of nodes of both pathways that are within a cutoff distance (7.5A) of one another. Using *overlap* as similarity metric, we clustered the pathways using the hierarchical clustering routine in MATLAB (The MathWorks, Natick, MA).

2.5. Comparison of allosteric pipelines across receptors

We calculated a similarity metric for each pair of pipelines among the different receptors, which is defined as the percentage of allosteric hubs that are common between the two pipelines. We then clustered the similar pipelines together using hierarchical clustering in MATLAB.

2.6. Convergence of MI

In proteins, correlated motion between allosteric residues can happen at all time scales, ranging from picoseconds to milliseconds or more. Here we are investigating allosteric correlation that happen in the sub-microsecond timescale. To test whether our simulations have sufficiently converged to capture equilibrium MI statistics, we calculated residue based MI by taking different lengths of the MD trajectories. We then compared the MI of a certain length of trajectory with that from a shorter trajectory by calculating the root mean square deviation between the two MI matrices (e.g. we calculated the RMSD between MI from 50 and 60 ns, then between 60 and 70 ns, and so on) (Figure. S1A). For all three trajectories, the MI RMSD rapidly decreased and stabilized around 70 ns. After 70 ns, any further increase in simulation time leads to little change in the magnitude of MI. This indicates that the simulations have converged.

2.7. Effect of the initial receptor structure on the observed allosteric behavior

To test whether the allosteric hubs depend on the initial receptor structure used in the MD, we performed ensembles of MD simulations starting from two different crystal structures of the inactive state of β_1AR (2Y03 and 4BVN). These two structures have subtle differences at the ends of the TM helices. Moreover, several loop residues are missing in one structure compared to the other. To eliminate the effect of the ligand, we used the same ligand norepinephrine in both simulations. The top allosteric hubs obtained from the two simulations were then compared to one another. Among the top 20 allosteric hubs, 70% of the residues were common between the two simulations as shown in Figure. S1B. Thus the starting receptor structure does not substantially affect the predicted allosteric hubs.

3. RESULTS AND DISCUSSION

3.1. β_2-adrenergic receptor shows the highest flexibility among the biogenic amine receptors

Figure. 1 shows the root mean square fluctuation (RMSF) per residue for every residue in each of the biogenic amine receptors. The X-axis label is the residue number using the

Ballesteros-Weinstein numbering system [19]. The loop residues are marked as ECL or ICL depending on extracellular loop or intracellular loop respectively. The calculated RMSF reflects the extent of flexibility of the residues in the GPCRs. The RMSF of the residues within the transmembrane (TM) regions stay within 1–3A, while the loop regions show higher RMSF > 6A. In order to quantify the flexibility of the TM domains, we plotted the average RMSF of the TM regions for each receptor (Figure. 1B). Among the six biogenic amine GPCRs studied here, β_2AR shows the highest RMSF, even from the closely related β_1AR. Detailed comparison of the RMSF among the TM regions shows that the increased RMSF of β_2AR comes mainly from TM6 and TM7 (Figure. 1C).

To understand the functional dynamics of the biogenic amine receptors in their inactive states, we measured the distribution of the distance between the IC ends of TM3 and TM6 as shown in Figure. 2. The antagonist or the inverse agonist bound receptors sample an ensemble of the microstates with higher population of receptor in the inactive state. Here, the TM3-TM6 distance is represented by the C_α-C_α distance between the highly conserved (among class A GPCRs) residues R3.50 and E6.30. These two residues are believed to form a salt bridge referred to as the 'ionic lock' in many GPCRs that stabilizes the inactive state [20]. The results for M_2R and M_3R are not included in Figure. 2 because the location of the residue 6.30 at the IC end of TM6 is unraveled in the M_2R crystal structure, [21], and this position is not resolved in the crystal structure of M_3R [22]. Among the other four receptors that we report, the two β adrenergic receptors show a bimodal TM3-TM6 distance distribution with two major peaks. One of the peaks is at a distance of 6A, which is shorter than the corresponding distance in the crystal structures of the β_1AR and β_2AR receptors (about 11A, pdb ID: 2VT4 [23] and 2RH1 [24]). This peak is in fact composed of three sub-peaks representing three closely related conformations (Figure. 2, red curve). The other peak is at 12–13A and is closer to the distance in the crystal structure of inactive β_2AR/β_1AR (11A). Also for each bin of the TM3-TM6 distance, The percentage of conformations that formed the ionic lock in each bin of the TM3-TM6 distance is shown as the area under the distribution curve (Figure. S2). While the left hand side peaks in the distance distributions of the adrenergic receptors show high ionic lock propensity, the right hand side peak (which is close to the inactive state crystal structure of β_2AR with the ionic lock) do not show any ionic lock. The other two receptors D_3R and H_1R show a single major peak at 7–8A similar to the inactive state crystal structures. While D_3R shows high ionic lock propensity throughout the TM3-TM6 distance distribution, H_1R shows weak ionic lock propensity. The wider distributions of TM3-TM6 distance in the two β adrenergic receptors correlate with their high basal activity [25].

The higher flexibility of β_2AR compared to the closely related β_1AR observed during the dynamics simulations is in agreement with the experimental observation that when both β_2AR and β_1AR were expressed in the same cell line, the basal activity of β_2AR was higher compared to β_1AR [25]. The high flexibility of β_2AR possibly facilitates the dynamics and its transition into an intermediate active-like state even in the absence of any agonist which explains it's elevated basal activity [1]. An observation of β_2AR sampling open conformations (increased TM3-TM6 distance) without a bound agonist was made previously in our simulations prior to experiments [2] and later also shown in NMR and DEER studies of the dynamics of β_2AR [1]. Among the six GPCRs, H_1R and M_3R show the least RMSF. However,

it should be noted that there is no experimental measurement comparing the basal activity of all the biogenic receptors except between β_2AR and β_1AR. All biogenic amine GPCRs show measurable levels of basal activity [25]. However our simulations indicate that among the receptors that we studied, the β adrenergic receptors tend to be more constitutively active compared to D_3R and H_1R. We note that given the complexity of the cellular environment, such comparison is only feasible when the different receptors are expressed in the same cell. The broader TM3-TM6 distance distribution in β_2AR is also in line with its high RMSF.

3.2. Reduced packing efficiency in the TM region leads to enhanced activation

To understand the dynamic behavior of GPCR conformations, we compared the packing efficiency of the residues in the TM domains among the different receptors during the MD simulations. Analysis of the crystal structures of some of the class A GPCRs showed that there is a cluster of hydrophobic residues in the middle of TM2, TM3 and TM6 (residues L3.43, F6.44, X6.40; X: I,L,V,M and X6.41), whose side chains are tightly packed in the inactive state crystal structures [26], and are disrupted in the active state crystal structures of β_2AR and M_3R. Moreover, some of these residues showed concerted side chain rearrangement during deactivation of β_2AR as observed in microsecond scale MD simulations [4a]. Thus it is proposed that the hydrophobic packing in the core of the TM region stabilizes the inactive state. Indeed, mutation of one of these residues F6.44 in β_2AR leads to a constitutively active mutant (CAM) [27]. Figure. 3A shows the net packing efficiency of the four hydrophobic residues in the MD simulations of the six biogenic amine receptors averaged over time. Among these receptors, β_2AR shows the lowest packing efficiency, while the M_2R and M_3R show the highest packing efficiency. The low packing efficiency of β_2AR will facilitate the disruption of the hydrophobic packing necessary for activation. The weak hydrophobic packing in β2AR is therefore indicative of its high basal activity [25]. Figure. 3B displays the packing efficiency between each pair of hydrophobic residues that have been shown to be tightly packed in the active state crystal structures. β_2AR shows weak packing between every pair of residues except 3.43 and 6.41 (Ballesteros-Weinstein numbering). Thus the weakened hydrophobic packing in β_2AR is a result of reduced packing involving the entire core of the TM domains rather than a specific region. This could lead to a more dynamic receptor interior that facilitates conformational change. PAR1, the peptide binding GPCR also shows weak hydrophobic packing efficiency similar to that of β_2AR (Figure. S5). The weak hydrophobic packing of PAR1 could be related to its high constitutive internalization in absence of agonists [28]. The packing efficiency in A_{2A}R is comparable to that of D_3R, but less than that of the muscarinic receptors. Due to the lack of experimental data on comparison of constitutive activity among multiple GPCRs, it is difficult to correlate our packing efficiency observations directly with experiments.

3.3. Water penetration into the TM regions and role in activation

During the dynamics simulations, water penetrated into the binding cavity and the core of the TM domains in all the eight receptors. Among the six biogenic amine receptors simulated here, the β-adrenoceptors (and M_2R) showed the highest number of water molecules within the TM regions, whereas the two G_q coupled receptors, H_1R and M_3R showed the lowest amount of water in the TM domain (Figure. 4A). To analyze the water penetration into the TM regions in more detail, we compared the regions of high water

occupancy (regions with the most frequent presence of water) within the TM domains of the six receptors. Figure. 4C–H show the regions with high (cutoff given in the Methods section) water occupancy for each receptor. For all receptors, the ligand binding cavity shows high hydration. The IC domains of the receptors also show regions of high water occupancy. However the hydrated IC regions are disconnected from the hydrated ligand binding pocket, possibly due to the presence of the tight packing among the hydrophobic cluster of residues in the middle of the TM regions. Thus, there is no continuous 'water wire' in the inactive state of the biogenic amine GPCRs. This observation is in agreement with the recent simulation findings for the inactive state of rhodopsin [29]. From Figure. 4A and C/D, the hydrated IC regions in the β-adrenergic receptors are larger in volume compared to the other receptors. The extra waters are present near the polar residues on TM7 (near the S259$^{7.46}$ and the NPxxY motifs, Figure. 4C–D). Although M_2R shows a high number of water molecules in the TM region, majority of the water is located near the ligand binding pocket and not in the IC regions (as opposed to the adrenergic receptors). Both muscarinic receptors show the lowest amount of water in the IC regions, whereas their ligand binding pockets are heavily hydrated (Figure. 4G–H). In keeping with these results, the muscarinic receptors also show the highest packing efficiency within the hydrophobic core of their TM regions (Figure. 3A), which contributes to the low hydration. The high hydration of the binding pockets of the muscarinic receptors could be due to the presence of the allosteric modulator binding region right above the orthosteric binding cavity [30]. This open region within the EC loops may favor diffusion of extra water into the orthosteric ligand binding cavity. We also compared the water rich TM region of the biogenic amine receptors to that of PAR1 and $A_{2A}R$ (Figure. S6). Both PAR1 and $A_{2A}R$ show less hydration of the TM regions compared to the biogenic amine receptors (Figure. S6B). In spite of the differences in hydration among the six receptors, they share several common residues that show greater likelihood of being hydrated in all the receptors. These residue positions are shown in Figure. 4B. Two residues (3.28 and 3.29) near the top of the orthosteric binding pocket show high hydration. The residue 3.28 is aromatic (Trp/Phe) in all six receptors. However the residue 3.29 is polar (threonine) in β adrenoceptors and hydrophobic (Leu/Val) in the other receptors. Despite being non-conserved in chemical character (polar vs. hydrophobic), the residue 3.29 is hydrated in all six receptors, which indicates that the water molecules near this residue could be functionally significant in the biogenic amine receptors. The region near the residue 3.35 at the bottom of the orthosteric cavity is also hydrated in all the receptors. This residue is not conserved among the six receptors. The region near the residue 3.35 forms the floor of the orthosteric ligand binding cavity, and is near the connector region [4a] that modulates allosteric communication between the agonist and G protein coupling domains [4b]. Thus, the presence of water in this region could have a functional role in the allosteric communication as well as the GPCR activation. The other region of common hydration is the NPxxY motif, which has been shown to be functionally important in class A GPCRs [31]. For example, in the crystal structure of active β_2AR, Y326$^{7.53}$ forms a water mediated hydrogen bond with Y219$^{5.58}$, which is proposed to stabilize the active state of β_2AR [32]. From our simulations, we find that the NPxxY is also hydrated in the inactive state of all the six biogenic amine receptors. The conserved aspartate D2.50 is located in the middle of TM2 in class A GPCRs. This residue when mutated to Asn or Ala leads to loss of agonist efficacy in many biogenic amine GPCRs [33]. Moreover, microseconds of MD simulations with adrenergic receptors

have shown that protonation of D2.50 stabilizes the ionic lock between R3.50 and E6.30 (D2.50 is deprotonated in all our simulations) [34]. Thus, D2.50 is a key residue that modulates the activation of biogenic amine receptors. In our simulations, D2.50 is located within the high water density region in all the receptors. While the hydration of this residue is high in β_2AR, β_1AR, D_3R and H_1R (5–8 water molecules within 5A), the hydration is relatively weaker in M_2R and M_3R (2 water molecules). The weak hydration of D2.50 in the muscarinic receptors could be due to the overall low water density within their TM domain. Since D2.50 is consistently hydrated in all the receptors, water could play a role in mediating the functional role of this residue in biogenic amine receptor activation.

3.4. Mutation points that produce CAMs and UCMs function as hubs of allosteric communication

In our previous work we had developed a computational method to calculate the allosteric communication pathways present in various conformational states of β_2AR [4b]. The allosteric communication pathways were calculated using the mutual information in torsional angles of residues from long time scale MD trajectories. When multiple allosteric communication pathways show significant overlap, we term these as allosteric pipelines. We term the residues in the allosteric pipelines as “allosteric hubs”. In this work we have used the same method to calculate and compare the allosteric communication pipelines in the inactive state of the six biogenic amine receptors. This will help us to understand the role of antagonist/inverse agonist in the allosteric communication between distant residues in the biogenic amine receptors. We find that certain regions of the receptors show a high density of allosteric communication pipelines that could be of functional significance in the receptor. We previously calculated the allosteric pipelines in the microsecond dynamics of various functional states of the β_2AR [4b]. In this work, we report that the allosteric communication pipelines that communicate between the EC and IC regions of β_2AR are conserved among the six biogenic amine receptors. Figure. 5A shows two of the major allosteric pipelines that are conserved among the biogenic amine receptors (rest of the conserved pipelines are shown in supplementary figure S3). Figure. 5A shows the two pipelines as red and blue patches respectively, while the pathways that belong to each pipeline are shown as red or blue lines. The red allosteric pipeline starts at the interface residues located between the ECL2 (extracellular loop 2) and EC end of TM2, traverses through the orthosteric ligand binding pocket and ends at the IC end of TM5 and TM6, where the G-protein couples to the receptor. The blue allosteric communication pipeline shown in Figure. 5A, traverses mostly through TM7 and communicates with helix 8. These two pipelines span the entire length of the TM domains in all the six receptors, and could play a major role in mediating allosteric communication between the ligand binding site and G protein interface. In the microsecond simulations of β_2AR, the red pipeline was found to be stronger (higher pathway population) in the inactive state compared to the agonist bound intermediate state or the nanobody bound active state [4b]. We also previously showed that the agonist bound β_2AR showed weak allosteric communication between the agonist binding site and the G-protein coupling site [4b]. Since the red allosteric communication pipeline shown in Figure. 5A is the strongest in the inactive state (stronger the allosteric communication, less dynamic is the receptor), it could play a role in stabilizing TM5 and TM6 in their inactive conformation. Likewise, the blue allosteric communication pathway in Figure. 5A, that traverses through TM7 in the

inactive state could stabilize TM7 in the inactive state. From the crystal structure of visual arrestin bound rhodopsin, it is known that arrestin forms distinct structural contacts with TM7 and helix 8 of rhodopsin (and possibly in other class A GPCRs)[35]. Likewise the strength of communication along the two allosteric pipelines spanning TM6 and TM7 could modulate the signaling through β-arrestin. However Since the β-arrestin bound structure is not known for biogenic amine receptors, it is difficult to discuss the role of allosteric communication in arrestin signaling. Two residues in the EC loops of β_2AR, E192^{ECL2} and K305^{ECL3}, form a salt bridge in the inactive state right above the orthosteric pocket [24]. These two residues along with several other residues form the termini (starting point) of allosteric communication in the red pipeline. NMR experiments showed that the salt bridge involving E192^{ECL2} and K305^{ECL3} is weakened upon activation [36]. Since the dynamic behavior of the initiators of allosteric communication (i.e. E192^{ECL2} and K305^{ECL3}) is experimentally connected to activation, it corroborates our computational findings.

The allosteric hub residues that are common to all the six biogenic amine receptors are shown as spheres in Figure. 5B. The sphere radius for each hub residue is proportional to the number of allosteric pathways going through that residue, called the hub strength. To investigate whether the allosteric hubs that are common to the biogenic amine receptors could also be conserved in other class A GPCRs, we calculated the allosteric hub score of these residue positions (by Ballesteros-Weinstein number) in, PAR1 and A_{2A}R. Both PAR1 and A_{2A}R are distant in their amino acid sequence similarity from any of the biogenic amine receptors [37]. We find that 54% of the allosteric hubs in the biogenic amine receptors are in the top 15% by allosteric hub score in either A_{2A}R or PAR1 (Figure. S7). Five of the hub residues are allosteric hubs in both A_{2A}R and PAR1. These residues are 2.39, 3.50, 5.61, 5.62 and 6.37 (Ballesteros- Weinstein number). These residues are thus important for allosteric communication in other class A GPCRs besides the biogenic amine receptors. In order to understand the role of the allosteric hubs in receptor activation, we collected experimental information on the mutations of these hub residues in biogenic amine receptors from the literature (table S1). We eliminated the mutations of residues that are in the ligand binding pocket, since their mutations could affect ligand binding affinity rather than allosteric communication. Many of the major allosteric hubs when mutated to alanine or other amino acids, decrease or enhance activation. Mutations that increase activation are referred to as CAMs (constitutively active mutants), while mutations that reduce or abolish activation are termed UCMs (uncoupling mutations) [38]. In Figure. 5B, the allosteric hubs whose mutations produce CAMs or UCMs are highlighted in green or red respectively. By comparing the strengths of allosteric hubs among the inactive, agonist bound and agonist/G protein bound active states of β_2AR, Bhattacharya et al. [4b] showed that the residues that produce CAMs upon mutation showed increased allosteric communication in the inactive state compared to the agonist bound or the G protein bound active state. Likewise, residues whose mutations produce UCMs showed weakened allosteric communication in the inactive state compared to the agonist bound or active states. Upon mutation of these allosteric hubs, the allosteric communication pipelines mediated by these residues are modulated possibly leading to a shift in conformational equilibrium between the inactive and the active states. This justifies the experimental mutation results, and validates our computational identification of the allosteric hubs as well.

In Figure. 5B, several residues in the ligand binding site act as major hubs of allosteric communication in all the six receptors. These residues include D3.32, which forms a salt bridge with the protonated nitrogen of the biogenic amine ligands, and residue 3.37 which is located below the ligand in the orthosteric ligand binding cavity. D3.32 is conserved among all biogenic amine receptors, whereas 3.37 is a threonine in all receptors except the muscarinic receptors where this residue is an asparagine, thus preserving a common polar character. These two residues could play a common role in biogenic amine receptors in mediating the signal of agonist/antagonist binding to the G protein interface. At the G protein interface, there are several major allosteric hubs, namely R3.50 and residue 2.39. These two residues directly interact with the C-terminus of $G_{s\alpha}$ in the active state structure of β_2AR [39]. Several major allosteric hubs are located in the IC regions of TMs 3, 5, 6, and 7, between the orthosteric ligand binding site and the G protein coupling interface. These residues act as intermediate nodes in communication between the orthosteric site and the G protein interface. Majority of these intermediate hubs that are conserved among the six biogenic amine receptors are sites of CAMs or UCMs in experiments. For example, in α_{1B}-adrenergic receptor, mutating S3.39 to alanine impaired G protein activation by 50% [40]. Mutating Y5.58 on TM5 to alanine thermostabilized β_1AR in the inactive state [41]. In α_{1B} adrenergic receptor, mutating L6.37 to alanine reduced G protein activation by 70% [42]. Also mutating N7.49 in the highly conserved NPxxY motif in β_2AR leads to loss of activation [31]. A few of the allosteric hubs also act as positions for CAMs. In β_2AR, mutating L3.43 to alanine increases G protein activation [43]. Also mutating L3.43 along with S3.47 to alanine increased basal activity in M_1R [44]. In M5R and α_{1B}AR, mutating the residue position 6.40 to Ser and Phe increased the receptor basal activity [27]. F6.44 is situated on TM6 below the highly conserved tryptophan of the WxP motif. Mutating this residue to various amino acids lead to constitutive activity in several biogenic amine receptors [27]. Overall, the experimental mutation data indicates that the allosteric hub residues in multiple biogenic amine receptors play significant role in the activation of these receptors.

3.5. Discussion

GPCRs are highly dynamic at room temperature and this dynamic nature allows them to couple to multiple intracellular proteins in the presence of various types of agonists, leading to functional selectivity. Also due their dynamic nature, many GPCRs also show significant basal activity in the absence of agonists. The results presented in this paper suggest that among the biogenic amine receptors, the β-adrenergic receptors are more dynamic compared to the other receptors in the inactive state. Both the adrenergic receptors subtypes studied here (β_1AR and β_2AR) show high RMSF, a broader TM3-TM6 distance distribution, loose packing efficiency within the hydrophobic core of the TMs and increased water penetration within the TM region. These observations corroborate with the high basal activity of the adrenergic receptors [25]. Both adrenergic receptors sample two distinct conformational ensembles, one with an inwardly collapsed IC end of TM6, and the other with a more open TM6 conformation (close to the β_2AR/β_1AR crystal structures) (Figure. S4A). In three of ten MD trajectories for the β_2AR, the receptor adopts an open conformation of TM6, similar to the inactive crystal structure (Figure. S4B & C). Upon exclusion of these three trajectories, the TM3-TM6 distribution of β_2AR shows only a single peak at short TM3-TM6 distance (Figure. S4D). Notably, this open conformation was not observed in the other

two receptors, D_3R and H_1R. In a recent work by Kobilka and coworkers, β_2AR was shown to exist in two distinct conformations in the inactive state, one with the ionic lock formed (state S1), and the other without the ionic lock (state S2) [1]. In our simulations of β_2AR, the left major peak in the TM3-TM6 distance distribution of β_2AR is comprised of three closely spaced peaks (Figure. 2). Two of these peaks show high propensity of the ionic lock being formed, while the third one shows less propensity for the ionic lock (Figure. S2B). The first two peaks could therefore represent the state S1, whereas the third peak could be state S2. It should be noted that the experimentally determined timescale for exchange between S1 and S2 is in the range of microseconds, and hence this transition is unlikely to be observed in a single MD trajectory in our simulations, which are 100 ns in length. Therefore the accuracy of the population distribution of the S1 and S2 states as obtained from our simulations is limited by the statistics available from the MD trajectories.

All six biogenic amine receptors show conserved allosteric pipelines communicating between the orthosteric ligand binding site and the G protein coupling interface. Conserved allosteric hub residues in these pipelines modulate the allosteric communication. Many of the conserved allosteric hubs are also involved in allosteric communication in two other class A GPCRs, PAR1 and $A_{2A}R$, that are distant from the biogenic amine receptors. This suggests a broader involvement of these allosteric hubs in the class A GPCR family. Experimentally mutating the allosteric hub residues affects receptor activation, by disrupting or enhancing the allosteric communication with the G protein interface and thus altering the equilibrium between the inactive and active states. Interestingly during the dynamics simulations, majority of the conserved allosteric hubs are involved in hydrogen bonds with water molecules within the transmembrane region in all the six receptors. The allosteric hubs which show the highest residence time of such hydrogen bonds include N1.50 on TM1, D2.50 on TM2, R3.50 on TM3 and multiple hubs on TM7 including the NPxxY motif. The other allosteric hubs are also involved in hydrogen bonds with water, but these hydrogen bonds are dynamic. The interaction of the allosteric hubs with water during the receptor dynamics suggests that water plays an important role in allosteric communication.

4. SUMMARY

In summary, we have shown that class A GPCRs that are more related in pharmacology have evolved to adopt a common mechanism of activation. This is signified by the common allosteric pipelines in all six biogenic amine receptors that mediate allosteric communication between the orthosteric site and EC loops to the G protein interface. Residues that function as major allosteric hubs in all six GPCRs are predicted to be involved in receptor activation. Indeed, a major percentage of these residues when mutated experimentally suppress or enhance activation, thus corroborating our hypothesis. In spite of the common mechanism of activation, the six GPCRs studied here show significant differences in their dynamic behavior, as shown by the differential packing of hydrophobic residues in the TM core, hydration of the TM regions, and fluctuations of the IC end of TM6. Among the six GPCRs, β_2AR shows the highest level of dynamic behavior in the inactive state, and is indicative of its high basal activity compared to closely related receptors such as the β_1AR. Many of the residue positions that serve as allosteric hubs in the biogenic amine receptors also act as allosteric hubs in two other class A GPCRs that are phylogenetically distant from the

biogenic amine family. The allosteric pipelines identified in this work are thus conserved in a larger group of class A GPCRs than just the biogenic amine receptors. These results therefore increase our understanding of the mechanism of activation of class A GPCRs.

Supplementary Material

Refer to Web version on PubMed Central for supplementary material.

Acknowledgments

This work was supported by National Institutes of Health [grant NIH-RO1-GM097261]. Participated in research design: SB, RSF, NV Conducted computations: RSF, SL Performed data analysis: SB, NV Wrote or contributed to the writing of the manuscript: SB, NV

References

1. Manglik A, Kim TH, Masureel M, Altenbach C, Yang Z, Hilger D, Lerch MT, Kobilka TS, Thian FS, Hubbell WL, Prosser RS, Kobilka BK. Cell. 2015; 161:1101–1111. [PubMed: 25981665]
2. Niesen MJ, Bhattacharya S, Vaidehi N. J Am Chem Soc. 2011; 133:13197–13204. [PubMed: 21766860]
3. (a) Kim TH, Chung KY, Manglik A, Hansen AL, Dror RO, Mildorf TJ, Shaw DE, Kobilka BK, Prosser RS. J Am Chem Soc. 2013; 135:9465–9474. [PubMed: 23721409] (b) Nygaard R, Zou Y, Dror RO, Mildorf TJ, Arlow DH, Manglik A, Pan AC, Liu CW, Fung JJ, Bokoch MP, Thian FS, Kobilka TS, Shaw DE, Mueller L, Prosser RS, Kobilka BK. Cell. 2013; 152:532–542. [PubMed: 23374348]
4. (a) Dror RO, Arlow DH, Maragakis P, Mildorf TJ, Pan AC, Xu H, Borhani DW, Shaw DE. Proc Natl Acad Sci U S A. 2011; 108:18684–18689. [PubMed: 22031696] (b) Bhattacharya S, Vaidehi N. Biophys J. 2014; 107:422–434. [PubMed: 25028884]
5. (a) Strader CD, Candelore MR, Hill WS, Sigal IS, Dixon RA. J Biol Chem. 1989; 264:13572–13578. [PubMed: 2547766] (b) Savarese TM, Wang CD, Fraser CM. J Biol Chem. 1992; 267:11439–11448. [PubMed: 1317867]
6. (a) Lee S, Bhattacharya S, Grisshammer R, Tate C, Vaidehi N. J Phys Chem B. 2014; 118:3355–3365. [PubMed: 24579769] (b) Soto AG, Smith TH, Chen B, Bhattacharya S, Cordova IC, Kenakin T, Vaidehi N, Trejo J. Proc Natl Acad Sci U S A. 2015; 112:E3600–3608. [PubMed: 26100877]
7. Sali A, Blundell TL. J Mol Biol. 1993; 234:779–815. [PubMed: 8254673]
8. Schuttelkopf AW, van Aalten DM. Acta Crystallogr D Biol Crystallogr. 2004; 60:1355–1363. [PubMed: 15272157]
9. Becke AD. J Chem Phys. 1993; 98:5648–5652.
10. Hess B, Kutzner C, van der Spoel D, Lindahl E. J Chem Theory Comput. 2008; 4:435–447. [PubMed: 26620784]
11. MacKerell AD, Bashford D, Bellott M, Dunbrack RL, Evanseck JD, Field MJ, Fischer S, Gao J, Guo H, Ha S, Joseph-McCarthy D, Kuchnir L, Kuczera K, Lau FTK, Mattos C, Michnick S, Ngo T, Nguyen DT, Prodhom B, Reiher WE, Roux B, Schlenkrich M, Smith JC, Stote R, Straub J, Watanabe M, Wiórkiewicz-Kuczera J, Yin D, Karplus M. J Phys Chem B. 1998; 102:3586–3616. [PubMed: 24889800]
12. Oostenbrink C, Villa A, Mark AE, Van Gunsteren WF. J Comp Chem. 2004; 25:1656–1676. [PubMed: 15264259]
13. Páll, S.; Abraham, M.; Kutzner, C.; Hess, B.; Lindahl, E. Tackling Exascale Software Challenges in Molecular Dynamics Simulations with GROMACS. In: Markidis, S.; Laure, E., editors. Solving Software Challenges for Exascale. Vol. 8759. Springer International Publishing; 2015. p. 3-27.
14. (a) Hoover WG. Phys Rev A. 1985; 31:1695–1697.(b) Nose S. J Chem Phys. 1984; 81:511–519.
15. Parrinello M, Rahman A. J Appl Phys. 1981; 52:7182–7190.

16. Essmann U, Perera L, Berkowitz ML, Darden T, Lee H, Pedersen LG. J Chem Phys. 1995; 103:8577–8593.
17. Humphrey W, Dalke A, Schulten K. J Mol Graph. 1996; 14:33–38. [PubMed: 8744570]
18. Dijkstra EW. Numerische Mathematik. 1959; 1:269–271.
19. Ballesteros, JA.; Weinstein, H. Integrated methods for the construction of three-dimensional models and computational probing of structure-function relations in G protein-coupled receptors. In: Stuart, CS., editor. Methods in Neurosciences. Vol. 25. Academic Press; 1995. p. 366-428.
20. Vogel R, Mahalingam M, Ludeke S, Huber T, Siebert F, Sakmar TP. J Mol Biol. 2008; 380:648–655. [PubMed: 18554610]
21. Haga K, Kruse AC, Asada H, Yurugi-Kobayashi T, Shiroishi M, Zhang C, Weis WI, Okada T, Kobilka BK, Haga T, Kobayashi T. Nature. 2012; 482:547–551. [PubMed: 22278061]
22. Kruse AC, Hu J, Pan AC, Arlow DH, Rosenbaum DM, Rosemond E, Green HF, Liu T, Chae PS, Dror RO, Shaw DE, Weis WI, Wess J, Kobilka BK. Nature. 2012; 482:552–556. [PubMed: 22358844]
23. Warne T, Serrano-Vega MJ, Baker JG, Moukhametzianov R, Edwards PC, Henderson R, Leslie AG, Tate CG, Schertler GF. Nature. 2008; 454:486–491. [PubMed: 18594507]
24. Cherezov V, Rosenbaum DM, Hanson MA, Rasmussen SG, Thian FS, Kobilka TS, Choi HJ, Kuhn P, Weis WI, Kobilka BK, Stevens RC. Science. 2007; 318:1258–1265. [PubMed: 17962520]
25. Milligan G. Mol Pharmacol. 2003; 64:1271–1276. [PubMed: 14645655]
26. Tehan BG, Bortolato A, Blaney FE, Weir MP, Mason JS. Pharmacol Ther. 2014; 143:51–60. [PubMed: 24561131]
27. Spalding TA, Burstein ES, Henderson SC, Ducote KR, Brann MR. J Biol Chem. 1998; 273:21563–21568. [PubMed: 9705286]
28. Soh UJ, Dores MR, Chen B, Trejo J. Br J Pharmacol. 2010; 160:191–203. [PubMed: 20423334]
29. Yuan S, Filipek S, Palczewski K, Vogel H. Nat Commun. 2014; 5:4733. [PubMed: 25203160]
30. Kruse AC, Ring AM, Manglik A, Hu J, Hu K, Eitel K, Hubner H, Pardon E, Valant C, Sexton PM, Christopoulos A, Felder CC, Gmeiner P, Steyaert J, Weis WI, Garcia KC, Wess J, Kobilka BK. Nature. 2013; 504:101–106. [PubMed: 24256733]
31. Barak LS, Menard L, Ferguson SS, Colapietro AM, Caron MG. Biochemistry. 1995; 34:15407–15414. [PubMed: 7492540]
32. Ring AM, Manglik A, Kruse AC, Enos MD, Weis WI, Garcia KC, Kobilka BK. Nature. 2013; 502:575–579. [PubMed: 24056936]
33. (a) Chung FZ, Wang CD, Potter PC, Venter JC, Fraser CM. J Biol Chem. 1988; 263:4052–4055. [PubMed: 2831218] (b) Fraser CM, Wang CD, Robinson DA, Gocayne JD, Venter JC. Mol Pharmacol. 1989; 36:840–847. [PubMed: 2557534] (c) Neve KA, Cox BA, Henningsen RA, Spanoyannis A, Neve RL. Mol Pharmacol. 1991; 39:733–739. [PubMed: 1828858]
34. Vanni S, Neri M, Tavernelli I, Rothlisberger U. Journal of Molecular Biology. 2010; 397:1339–1349. [PubMed: 20132827]
35. Kang Y, Zhou XE, Gao X, He Y, Liu W, Ishchenko A, Barty A, White TA, Yefanov O, Han GW, Xu Q, de Waal PW, Ke J, Tan MH, Zhang C, Moeller A, West GM, Pascal BD, Van Eps N, Caro LN, Vishnivetskiy SA, Lee RJ, Suino-Powell KM, Gu X, Pal K, Ma J, Zhi X, Boutet S, Williams GJ, Messerschmidt M, Gati C, Zatsepin NA, Wang D, James D, Basu S, Roy-Chowdhury S, Conrad CE, Coe J, Liu H, Lisova S, Kupitz C, Grotjohann I, Fromme R, Jiang Y, Tan M, Yang H, Li J, Wang M, Zheng Z, Li D, Howe N, Zhao Y, Standfuss J, Diederichs K, Dong Y, Potter CS, Carragher B, Caffrey M, Jiang H, Chapman HN, Spence JC, Fromme P, Weierstall U, Ernst OP, Katritch V, Gurevich VV, Griffin PR, Hubbell WL, Stevens RC, Cherezov V, Melcher K, Xu HE. Nature. 2015; 523:561–567. [PubMed: 26200343]
36. Bokoch MP, Zou Y, Rasmussen SG, Liu CW, Nygaard R, Rosenbaum DM, Fung JJ, Choi HJ, Thian FS, Kobilka TS, Puglisi JD, Weis WI, Pardo L, Prosser RS, Mueller L, Kobilka BK. Nature. 2010; 463:108–112. [PubMed: 20054398]
37. (a) Fredriksson R, Lagerstrom MC, Lundin LG, Schioth HB. Mol Pharmacol. 2003; 63:1256–1272. [PubMed: 12761335] (b) Stevens RC, Cherezov V, Katritch V, Abagyan R, Kuhn P, Rosen H, Wuthrich K. Nat Rev Drug Discov. 2013; 12:25–34. [PubMed: 23237917]

38. Rosenbaum DM, Cherezov V, Hanson MA, Rasmussen SG, Thian FS, Kobilka TS, Choi HJ, Yao XJ, Weis WI, Stevens RC, Kobilka BK. Science. 2007; 318:1266–1273. [PubMed: 17962519]
39. Rasmussen SG, DeVree BT, Zou Y, Kruse AC, Chung KY, Kobilka TS, Thian FS, Chae PS, Pardon E, Calinski D, Mathiesen JM, Shah ST, Lyons JA, Caffrey M, Gellman SH, Steyaert J, Skiniotis G, Weis WI, Sunahara RK, Kobilka BK. Nature. 2011; 477:549–555. [PubMed: 21772288]
40. Cavalli A, Fanelli F, Taddei C, De Benedetti PG, Cotecchia S. FEBS Lett. 1996; 399:9–13. [PubMed: 8980109]
41. Serrano-Vega MJ, Magnani F, Shibata Y, Tate CG. Proc Natl Acad Sci U S A. 2008; 105:877–882. [PubMed: 18192400]
42. Greasley PJ, Fanelli F, Rossier O, Abuin L, Cotecchia S. Mol Pharmacol. 2002; 61:1025–1032. [PubMed: 11961120]
43. Tao YX, Abell AN, Liu X, Nakamura K, Segaloff DL. Mol Endocrinol. 2000; 14:1272–1282. [PubMed: 10935550]
44. Rosenau A, Cattier B, Gousset N, Harriau P, Philippon A, Quentin R. Antimicrob Agents Chemother. 2000; 44:760–762. [PubMed: 10681352]

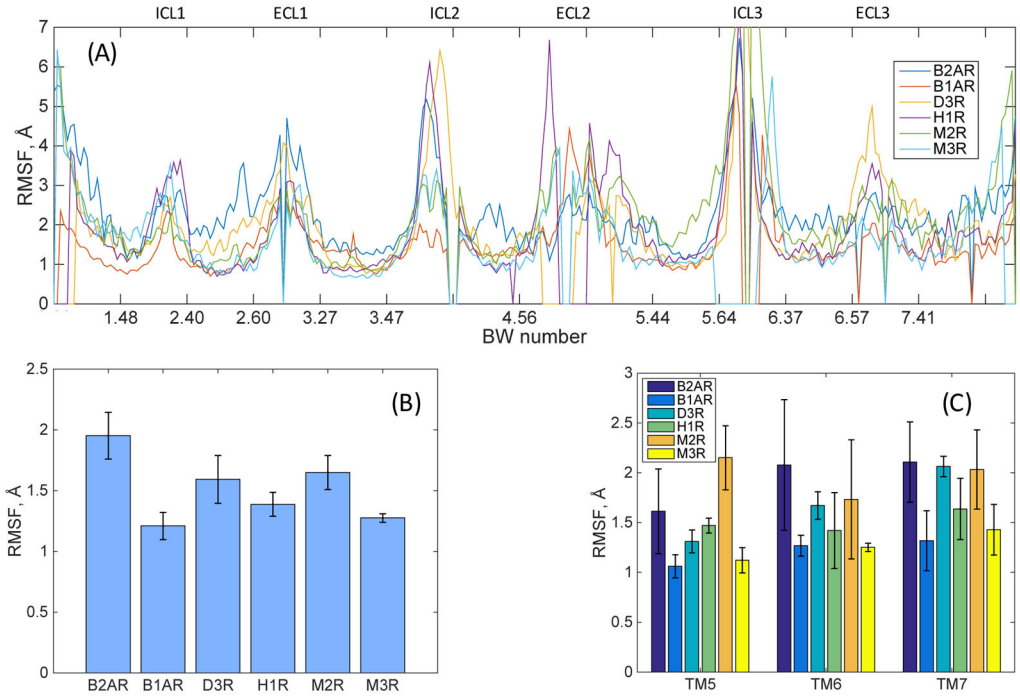

Figure 1.

(A) Root mean square fluctuation (RMSF) per residue for different biogenic amine receptors; (B) average RMSF of each receptor; (C) average RMSF by TM region; the error bars represent 95% confidence limits.

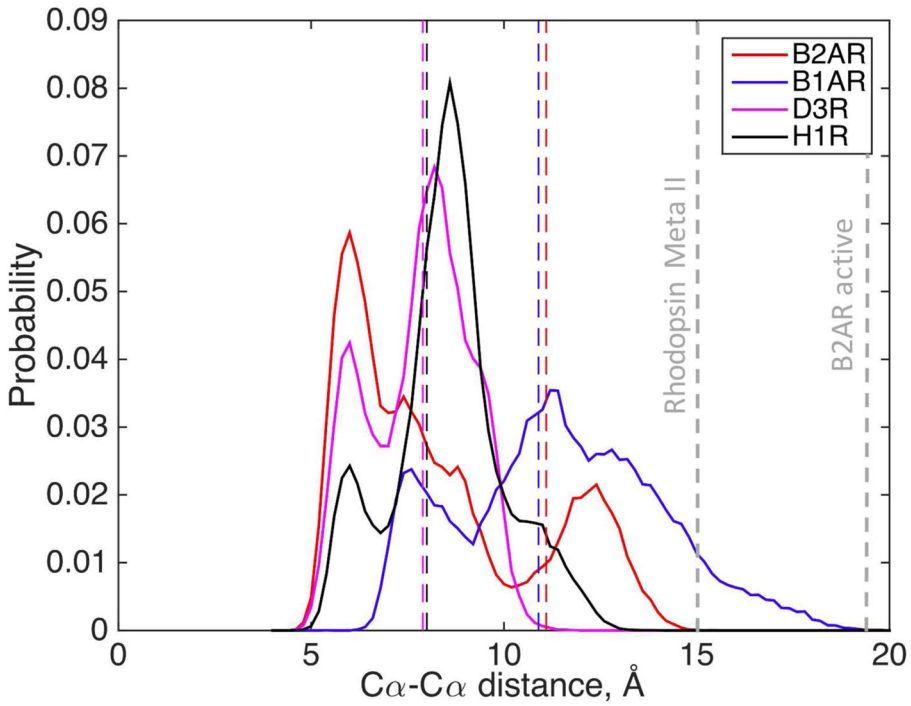

Figure 2.

Distribution of TM3-TM6 distance (between R3.50 and residue at position 6.30) observed during the dynamics of the different GPCRs. The colored vertical lines represent the respective crystal structure distances (color coded according to figure legend). The grey vertical lines denote the corresponding distances in active state crystal structures

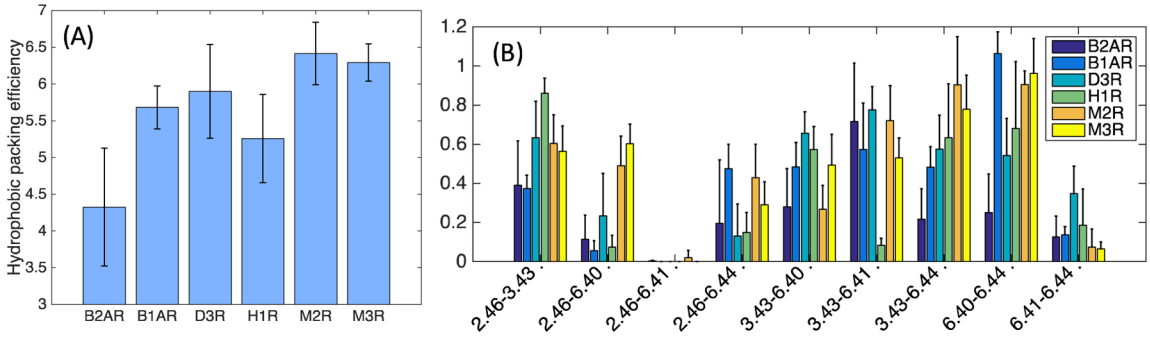

Figure 3.

(A) Interhelical residue packing efficiency among the hydrophobic residues in the middle of TM2, TM3 and TM6 as observed during the dynamics of different biogenic amine receptors; (B) packing efficiency for each inter-residue contact enumerated in [26]; the error bars represent 95% confidence limits; for simplicity, only the upper bounds are highlighted in (B).

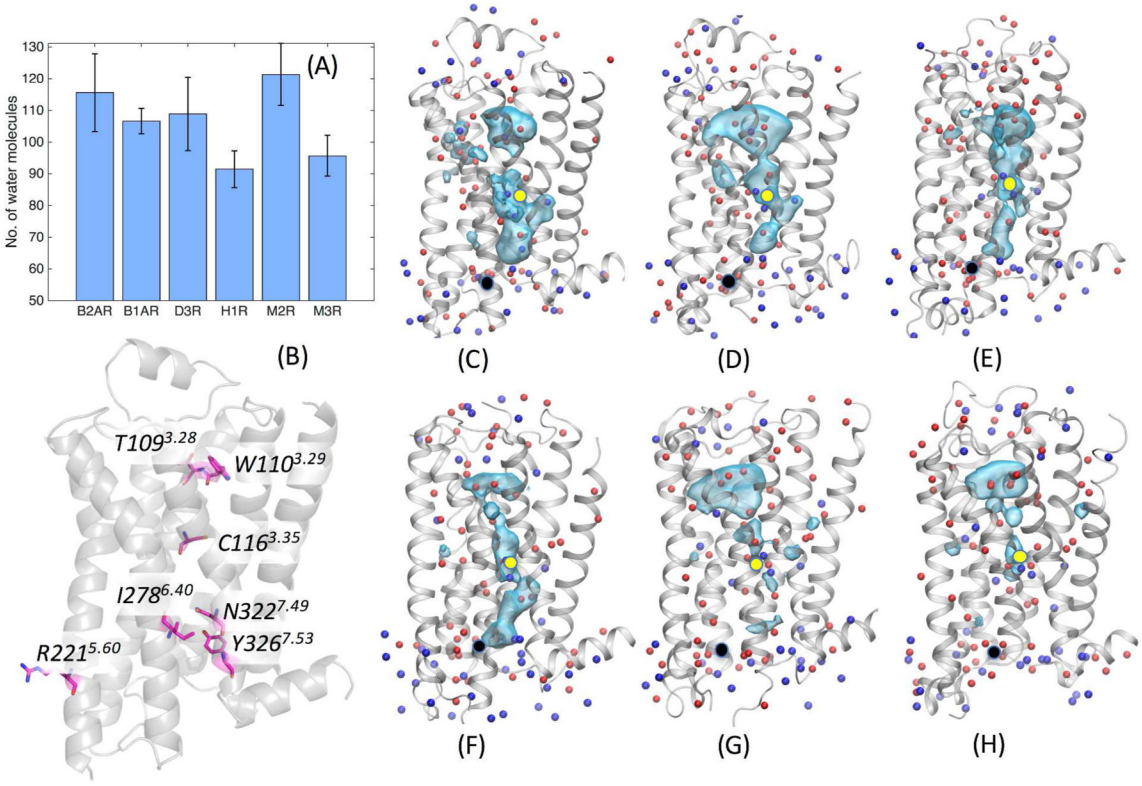

Figure 4.

(A) Average number of water molecules within 5A of functional hotspots (residues that are involved in activation of class A GPCRs); the error bars represent 95% confidence limits. (B) common residues that show presence of water in all biogenic amine receptors; the residues numbers are from β_2AR (C-H) regions of high water occupancy within the TM domains of the six GPCRs; C: β_2AR; D: β_1AR; E: D_3DR; F: H_1R; G: M_2R; H: M_3R; the sidechain atoms with OH/H groups that are exchangeable with water are shown as red (Ser, Thr, Tyr, Asp, Glu) and blue (Asn, Gln, Lys, Arg) spheres. The location of the residues D2.50 and R3.50 are highlighted as yellow and black circles respectively.

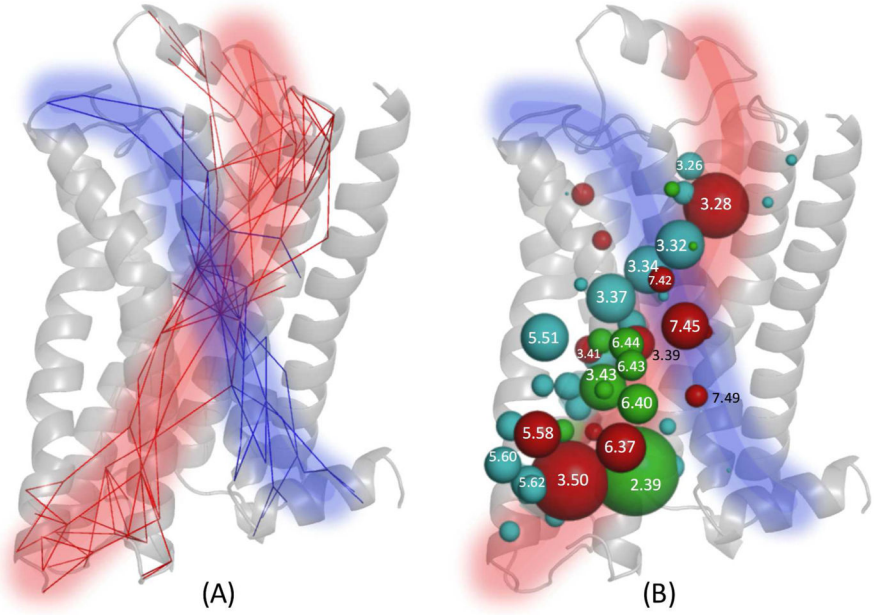

Figure 5.

(A) Top scoring two major allosteric pipelines calculated from the MD trajectories of the six biogenic amine receptors. These two pipelines connect the residues in the EC region to those in the G protein interface; the pipelines are shown in transparent colors, and the underlying clusters of allosteric pathways are shown as lines. These pipelines having varying strength among different receptors and also in different conformational states of the same receptor; (B) The allosteric hubs calculated for all the allosteric pipelines and those that are conserved among the biogenic amine receptors are shown as spheres; the radius of the spheres are proportional to the average strength of allosteric communication mediated by each of these residues; the allosteric hubs that are UCMs or CAMs in one or more receptors are highlighted in red and green respectively.